Decentralized Feedback Structures of a Vapor Compression Cycle System

Neera Jain, Bin Li, Michael Keir, Brandon Hencey, and Andrew Alleyne

***Abstract*—In vapor compression cycle systems, it is desirable to effectively control the thermodynamic cycle by controlling the thermodynamic states of the refrigerant. By controlling the thermodynamic states with an inner loop, supervisory algorithms can manage critical functions and objectives such as maintaining superheat and maximizing the coefficient of performance. In practice, it is generally preferred to tune multiple single-input–single-output (SISO) control inner loops rather than a single multiple-input–multiple-output control inner loop. This paper presents a process by which a simplified feedback control structure, amenable to a decoupled SISO control loop design, may be identified. In particular, the many possible candidate input–output (I/O) pairs for decentralized control are sorted via a decoupling metric, called the relative gain array number. From a reduced set of promising candidate I/O pairs, engineering insight is applied to arrive at the most effective pairings successfully verified on an experimental air-conditioning-and-refrigeration test stand.**

***Index Terms*—Air conditioning, decoupling, decentralized, HVAC, multivariable control, refrigeration.**

I. Introduction

THE PRIMARY goal of any air-conditioning or refrigeration system is to move energy from one location to another. An idealized vapor compression cycle (VCC) system, as shown in Fig. 1, is a thermodynamic system driven by the phase characteristics of the refrigerant that is flowing through it. Therefore, it is useful to describe the system in terms of the state of its refrigerant, as shown on a pressure–enthalpy ($P-h$) diagram (see Fig. 2).

An ideal VCC system assumes isentropic compression, isenthalpic expansion, and isobaric condensation and evaporation. The basic control objectives of a VCC system can be conceptualized visually via Fig. 2. For example, the difference between h_1 and h_4 represents the increase in enthalpy across the evaporator, i.e., the amount of energy (Q) removed from the cooled space. This is a measure of evaporator capacity. The difference between h_2 and h_1 represents the increase in enthalpy across the compressor, i.e., the amount of work (W) done by the compressor to increase the pressure of the refrigerant vapor. The system coefficient of performance (COP), a measure of system efficiency, is defined as the ratio between these two changes in enthalpy

$$COP = \frac{Q}{W} = \frac{h_1 - h_4}{h_2 - h_1}. \tag{1}$$

Rather than explicitly controlling capacity or efficiency, however, this paper aims to control the individual thermodynamic states of the system. Given the assumptions made for an ideal VCC system and the constitutive relationships between pressure, temperature, and enthalpy (i.e., for a given point on the cycle in Fig. 2, only two thermodynamic states are required to derive the remaining states for that point), only four thermodynamic states are needed to uniquely define the four points of the idealized cycle. This suggests that, with an appropriate control architecture, these four points of the VCC could be placed by a higher level planning algorithm [6], [7] so as to achieve an optimal balance between desired capacity and efficiency (see Fig. 3). This is a shift from the current practice where the actuators are used to meet specific control objectives. For example, in [2], the compressor is used to control capacity and the expansion valve is used to control evaporator superheat.

Vapor compression systems are closed cycles, implying strongly coupled system dynamics which arise from the effect of inputs essentially "feeding back" through the cycle. It has been shown that multivariable control techniques [1]–[3] can be used to handle input–output (I/O) couplings while achieving desired performance objectives. In [2], the system superheat and evaporator saturation temperature were used as the measured outputs supplied to an optimal observer to estimate the system states in a Linear Quadratic Gaussian approach. However, for industrial practitioners and service engineers, it is generally preferred to tune multiple single-input–single-output (SISO) control loops rather than a single multiple-input–multiple-output (MIMO) control loop. Designing a decentralized controller consisting of SISO control loops is greatly simplified when the interaction among the individual SISO control loops is sufficiently minimized.

Numerous control schemes have been developed with superheat and evaporation temperature (or pressure) as the feedback signals [1]–[4]. These references frequently noted the difficulty of controlling the two outputs with individual SISO control loops due to the physical coupling between superheat and evaporation temperature. Most recently, Keir and Alleyne [5] suggested that a novel choice of output control variables can decouple dynamics such that a decentralized control approach can be used to meet desired performance objectives. Specifically, the difference between the condenser and evaporator pressure was shown to be more effective as a feedback variable than evaporator pressure alone.

As motivated by the results in [5], this paper focuses on providing a structured method for determining control I/O pairs which effectively decouple system dynamics and allow the use

Manuscript received April 22, 2008. Manuscript received in final form November 26, 2008. First published April 28, 2009; current version published December 23, 2009. Recommended by Associate Editor S. Palanki. This work was supported in part by the sponsoring companies of the Air-Conditioning and Refrigeration Center at the University of Illinois at Urbana–Champaign and in part by Thermo King Corporation.

The authors are with the Mechanical Science and Engineering Department, University of Illinois, Urbana–Champaign, IL 61801 USA (e-mail: njain2@illinois.edu; binli2@illinois.edu; mckeir@gmail.com; bhencey@gmail.com; alleyne@illinois.edu).

Digital Object Identifier 10.1109/TCST.2008.2010500

1063-6536/$26.00 © 2009 IEEE

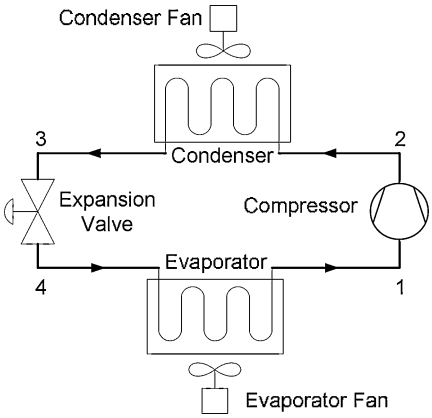

Fig. 1. Schematic of ideal subcritical vapor compression system.

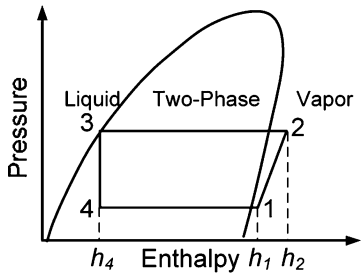

Fig. 2. $P-h$ diagram for ideal subcritical VCC.

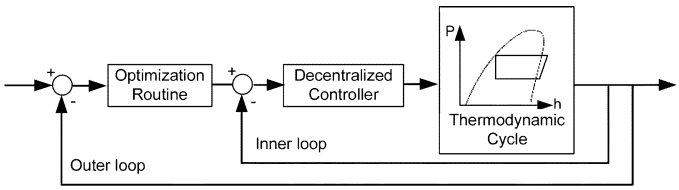

Fig. 3. Block diagram visualization of decentralized controller within a larger optimization control loop.

of a decentralized control approach. The output thermodynamic states considered for the control I/O pair analysis are derived from the four points of the idealized cycle as plotted on a $P-h$ diagram (Fig. 2). This enables the control designer to use an understanding of thermodynamics to shape the cycle to meet desired performance and efficiency objectives. Section 2 introduces the choice of candidate input control variables and output thermodynamic states and describes the generation of identified models used for the ensuing analysis. The next section describes the use of a decoupling metric to sort through candidate I/O pairings. A discussion of the analytical results and the role of engineering insight in further narrowing the field of candidate I/O pairings to a final set are presented in Section 4. Finally, Section 5 compares a chosen I/O set to a baseline I/O set (based on [1] and [2]) by comparing the performance of the respective decentralized proportional–integral–derivative (PID) controllers for both I/O sets.

II. System Modeling and Identification

A representative system model is required to understand which aspects of the thermodynamic cycle are best controlled

TABLE I
Nominal Operating Conditions for Experimental System

Output	P_1=P_4	P_2=P_3	T_1	T_2	T_3	T_4
Units	*kPa*	*kPa*	*C*	*C*	*C*	*C*
Nominal Condition	285	955	19.5	62.5	36.9	1.0

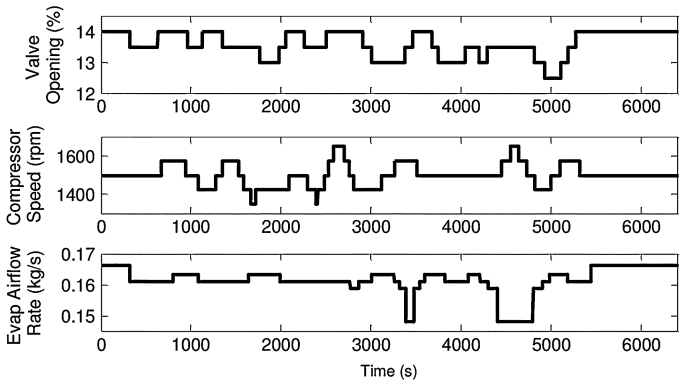

Fig. 4. Random Gaussian input signals.

by which input parameter. In this section, the dynamic response of a VCC system is identified using a time-domain-system identification procedure. Three controllable inputs for a variable-speed VCC are considered: expansion valve opening (u_1), compressor speed (u_2), and evaporator airflow rate (u_3). The condenser airflow rate is considered a disturbance to the system because, in some applications, e.g., automotive systems, the condenser airflow rate is a function of vehicle speed and, therefore, is not controlled.

The output measurements consist of six thermodynamic states: two pressures and four temperatures. Recall from Fig. 2 that, for an idealized cycle, there are two system pressures: $P_2 = P_3$ and $P_1 = P_4$. These correspond to the pressure inside the condenser and the pressure inside the evaporator, respectively. There are four system refrigerant temperatures: T_1, T_2, T_3, and T_4. Again, assuming an idealized cycle with a saturated refrigerant leaving the condenser, these represent evaporator outlet temperature, condenser inlet temperature, condenser saturation temperature, and evaporator saturation temperature, respectively.

The output responses to random Gaussian combinations of all three inputs (see Fig. 4) around a set of nominal operating conditions (shown in Table I), were collected on an air-conditioning-and-refrigeration experimental test stand. For a more detailed description of the experimental system, see [4] and [5].

A standard prediction error/maximum likelihood system identification algorithm from the Matlab System Identification Toolbox [8] was used to identify the frequency response between each input and output pair. Because system identification is sensitive to scaling, two models were identified, wherein the output parameters within each model shared the same units. That is, the first model was identified with all three excited inputs and the two pressure measurements as outputs ($P_2 = P_3$ and $P_1 = P_4$), and a second model was identified with the same inputs and the four temperature measurements as outputs

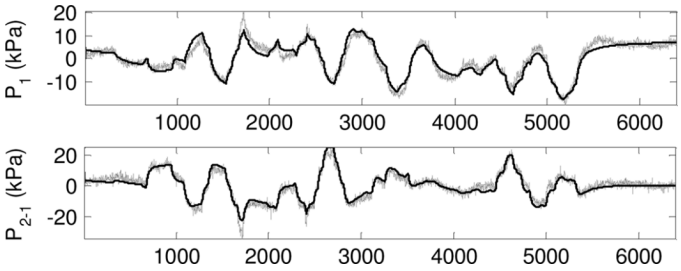

Fig. 5. System ID results for P_1 : fit $= 69.9\%$; P_{2-1} : fit $= 71.25\%$.

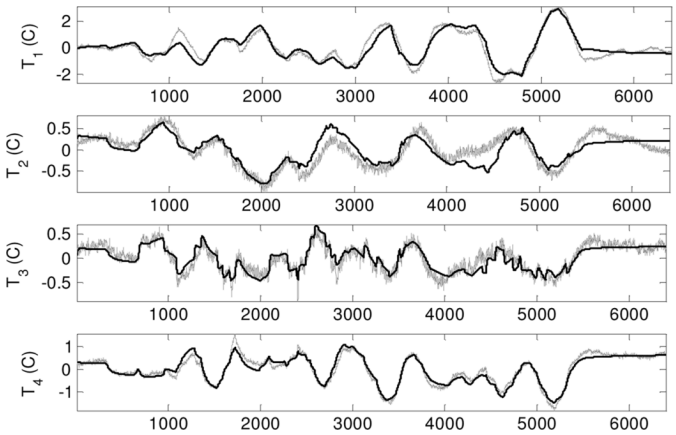

Fig. 6. System ID results for T_1 : fit $= 65.22\%$. T_2 : fit $= 43.99\%$. T_3 : fit $= 54.62\%$. T_4 : fit $= 72.81\%$.

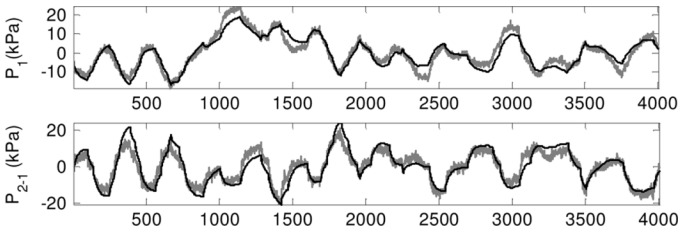

Fig. 7. Cross-validation of ID model for system pressures. P_1 : fit $= 65.63\%$. P_{2-1} : fit $= 55.92\%$.

(T_1, T_2, T_3, and T_4). The complete state-space representation of each identified model is included in Appendix A. Note that using $P_{2-1} \triangleq P_2 - P_1$ instead of P_2 provided a better fit with respect to the system identification.

For each identified output, the open-loop system response is compared against the response as predicted by the identified model. Figs. 5 and 6 show the identified model compared against the data used for the identification.

The identified models were then cross-validated using data collected on a different day with a different ambient temperature and humidity level (Figs. 7 and 8). The fit percentages for each output characterizing predictive capability of the models are included in the captions of each figure. Only the frequency response between each I/O pair is needed for the decoupling analysis, thereby allowing the flexibility to identify two separate models rather than a single three-input–six-output model.

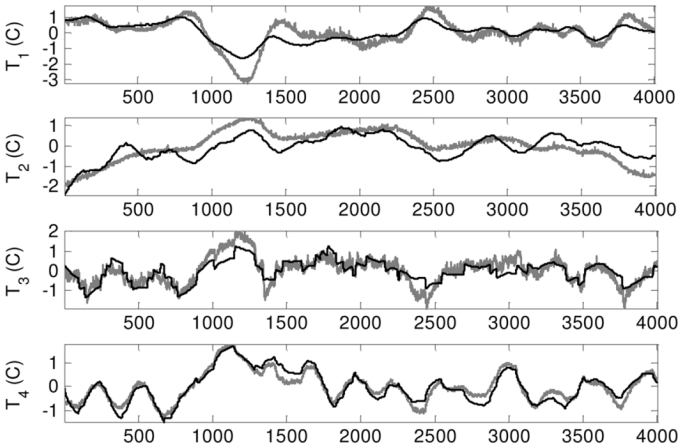

Fig. 8. Cross-validation of ID model for system temperatures. T_1 : fit $= 44.64\%$. T_2 : fit $= 34.4\%$. T_3 : fit $= 44.07\%$. T_4 : fit $= 63.72\%$.

III. I/O Pairing Analysis

Determining the *best* I/O pairs for a decoupled controller design involves considering a very large set of possible pairings. The following section applies a model-based decoupling metric to the aforementioned identified models in order to reduce the set to the most promising I/O pairs.

A. Output Combinations

For an idealized VCC, the output measurements T_1, T_2, T_3, T_4, $P_2 = P_3$, and $P_1 = P_4$ may be used to fully characterize the thermodynamic states of the cycle. However, other physically meaningful aspects of the cycle, such as evaporator superheat ($T_1 - T_4$), may present opportunities for further decoupling. In fact, there are an infinite number of affine output measurement combinations, represented by

$$\tilde{y} = \sum_{i=\{1,2\}} \alpha_i P_i + \sum_{i=\{1,2,3,4\}} \beta_i T_i \tag{2}$$

for some $\alpha_i, \beta_i \in \mathbb{R}$, that could be considered. Even though such affine combinations could be used to thoroughly decouple the individual identified loops, they are not necessarily physically meaningful in terms of the VCC. For example, the inverse and singular value decomposition of the frequency response of the system at a frequency ω, represented by the matrix $G(j\omega)$, could be used to determine affine combinations that decouple the individual loops at a frequency ω, but such combinations are sensitive to the choice of input and output scaling [10] and disregard the physical significance and units of the resulting combinations. In (2), the units of $\tilde{y} = \alpha_1 P_1 + \beta_1 T_1$ are ambiguous, and the simple addition of pressure and temperature does not carry any particular physical significance. For this investigation, each output is defined as a binary combination of either the temperatures or pressures, representing differences and averages, such as evaporator superheat or pressure differential. Each output combination $\tilde{y}$ takes the form of (2), where $(\beta_i = 0, \alpha_i = \{-1, 0, 1\})$ or $(\beta_i = \{-1, 0, 1\}, \alpha_i = 0)$. The possible binary combinations (2) for either two pressures or four temperatures are $\sum_{i=1}^{2} 3^{(i-1)} = 4$ and $\sum_{i=1}^{4} 3^{(i-1)} = 40$, respectively. Consequently, there are $44!/(44-3)! = 76\,464$ possible I/O pairs.

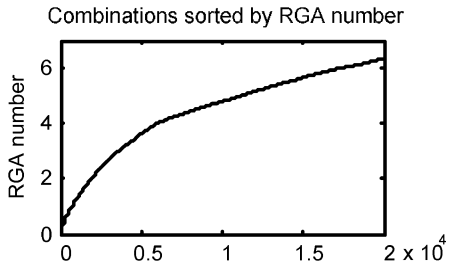

Fig. 9. Variation of RGA number for the best 20 000 (of 76464) candidates for three inputs for $\omega = 0$ rad/s.

B. Sorting via a Decoupling Metric

Given there are over 75 000 possible I/O pairings, it is essential that a decoupling metric be used to filter through the large number of possibilities. One metric that can be used to quantify the reduction in coupling provided by using one I/O pair over another is the relative gain array (RGA) technique originally developed by Bristol [9]. The technique is independent of input and output scaling, thereby avoiding the question of appropriate scaling of inputs and outputs with different magnitudes. For a nonsingular square matrix P, the RGA is defined by (3), where $\times$ denotes the Schur product

$$RGA(P) = \Lambda(P) = P \times (P^{-1})^{\mathrm{T}}. \tag{3}$$

The RGA is a good indicator of sensitivity to uncertainty in the input channels, diagonal dominance for state-space systems, and stability levels of decentralized controller designs [10].

Uncertainty in the input channels is indicated by plants with large RGA elements around the crossover frequency, making these plants fundamentally difficult to control. At a particular frequency ω, a measure of the diagonal dominance of a plant G is obtained by calculating the RGA number, given by

$$RGA\ number(G(j\omega)) = \|\Lambda(G(j\omega)) - I\|_{\mathrm{sum}} \tag{4}$$

where $\|M\|_{\mathrm{sum}}$ for some square matrix $M \in \mathbb{R}^{n\times n}$ is defined as $\sum_{i=1}^{n}\sum_{j=1}^{n}|m_{ij}|$.

Large RGA numbers are a clear indicator that the closed-loop performance will be poor when decentralized control schemes are applied [10]. The best achievable RGA number is 0.076 for the system identified in Section 2. As shown in Fig. 9, the RGA number varies smoothly with respect to the sorted candidate pairs, thereby suggesting that many pairings could prove nearly as effective as the "best" pairing.

IV. Comparison of Coupling for Different I/O Pairings

By applying the RGA number as a decoupling metric, the control designer is presented with a reduced field of the best potential I/O pair candidates. Subsequently, physical intuition is applied to further narrow the field for experimental trials. The following tables characterize how often each output was associated with an input u_i for the top 1000 I/O pairs, as characterized by the RGA number, at two different frequencies. The sums and differences of the outputs are condensed for compactness by applying notation of the form $P_{3-4} \triangleq P_3 - P_4$ and $T_{2+3+4} \triangleq T_2+T_3+T_4$. Note that the tables only present the top recurring outputs coupled to each input; therefore, the rows do not necessarily total to 100%. Moreover, recall that u_1, u_2, and u_3 represent electronic expansion valve (EEV) opening, compressor speed, and evaporator airflow rate, respectively.

TABLE II
Incidence of Candidate Output Pairings for u_1 for Top 1000 Pairings

Frequency	P_2=P_3	T_3	P_{3+4}	T_{2+3+4}
ω=0 rad/s	51%	19%	8%	5%
ω=0.01 rad/s	19%	4%	21%	7%

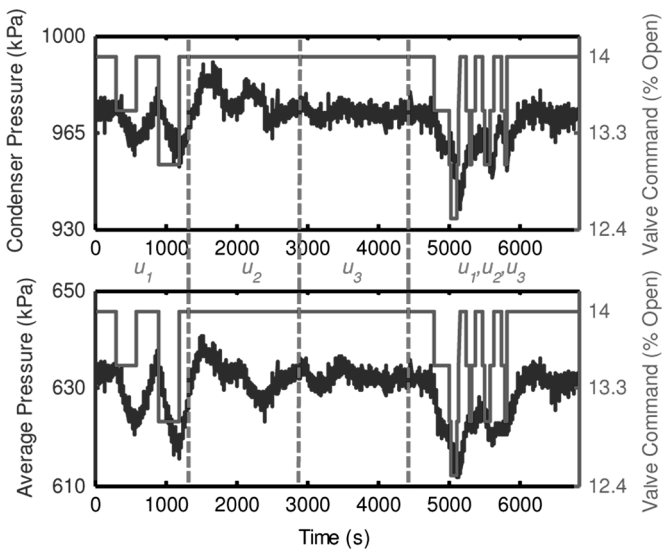

Fig. 10. Open-loop response of I/O coupling for input u_1.

Table II suggests that the EEV, input u_1, most strongly drives the condenser pressure $P_2(= P_3)$ particularly at low frequencies. Condenser saturation temperature T_3 is also driven by the EEV, but not as strongly as P_3. While it may seem redundant to consider both temperature and pressure at a saturated condition, Table II provides a strong motivation to do so. Pressure transducers are able to more accurately capture refrigerant dynamics than both immersion and wall-type thermocouples due to the higher signal bandwidth of pressure over temperature. This clearly plays a role when choosing decoupled I/O pairings.

Fig. 10 shows a qualitative metric for assessing how strongly u_1 drives each of these candidate output states. The experimental system was perturbed with a series of step changes in each input; here, we show a particular output state against only one input signal at a time to more clearly assess the coupling between that I/O pair.

The pairing of $P_2 = P_3$ with u_1 agrees with the intuition that the EEV controls the refrigerant mass flow rate leaving the condenser. Oftentimes, the EEV is used to regulate the evaporator superheat T_{1-4} because the electronic expansion valve is viewed as a programmable version of a thermal expansion valve [11]. Consequently, the regulation of the condenser pressure via the EEV runs counter to the typical VCC control design practice. Gaining potentially unconventional insights is one of the benefits of sorting through such a large set of I/O pairings.

TABLE III
INCIDENCE OF CANDIDATE OUTPUT PAIRINGS FOR u_2 FOR TOP 1000 PAIRINGS

Frequency	T_{-2-3+4}	T_{2-4}	T_{3-4}	P_{3-4}
ω=0 rad/s	17%	11%	8%	11%
ω=0.01 rad/s	21%	9%	13%	30%

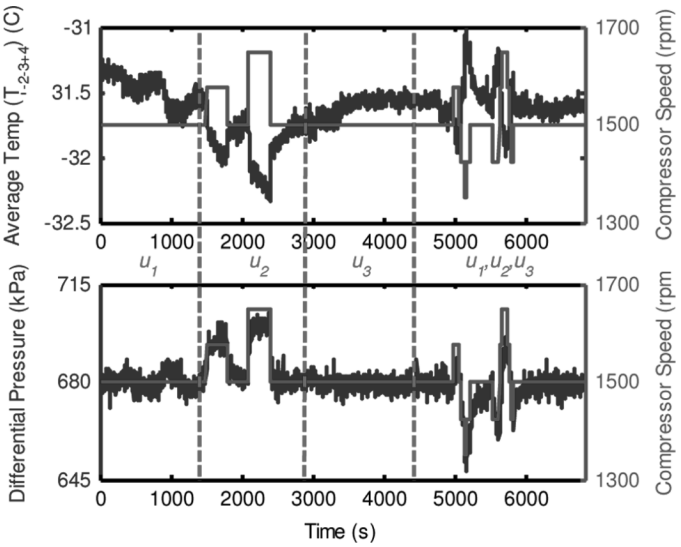

Fig. 11. Open-loop response of I/O coupling for input u_2.

Table III suggests that the compressor speed, input u_2, is tightly coupled with a combination of system temperatures T_{-2-3+4} and the difference between condenser and evaporator pressure P_{3-4}. In particular, the RGA analysis suggests that u_2 is more strongly coupled with T_{-2-3+4} at low frequencies but that, at higher frequencies, it drives P_{3-4}.

Fig. 11 shows that there is a strong correlation between the frequency-based RGA analysis and the open-loop responses. The pressure differential pairing P_{3-4} was originally demonstrated to significantly improve the performance of the decentralized two-input–two-output closed-loop system in [5]. However, the introduction of a third SISO loop presents new challenges with respect to decoupling.

Table IV suggests that the evaporator airflow rate u_3 drives some combination of the four temperatures. Both the evaporator outlet and saturation temperatures consistently appear in the most prominent combinations in Table IV, suggesting that T_{1+4} may be a good candidate. From Fig. 12, both T_{1+4} and $T_{1+2+3+4}$ appear to respond similarly to perturbations in u_3. From the perspective of the VCC, controlling the average evaporator refrigerant temperature T_{1+4} would, in effect, allow the control designer to regulate other aspects of the VCC of interest, such as the evaporator superheat.

With the field of possible I/O pairings narrowed down to two candidate outputs for each input, one final metric is needed to better understand if one I/O pair provides an advantage over another. Given that the RGA analysis is frequency dependent, it is important to more closely examine how the coupling between each I/O pair varies with respect to frequency. Tables II, III, and IV suggested that certain output states were more strongly coupled at either low frequencies or frequencies, but not necessarily both. Table V lists two possible sets y_1 and y_2 of I/O pairings.

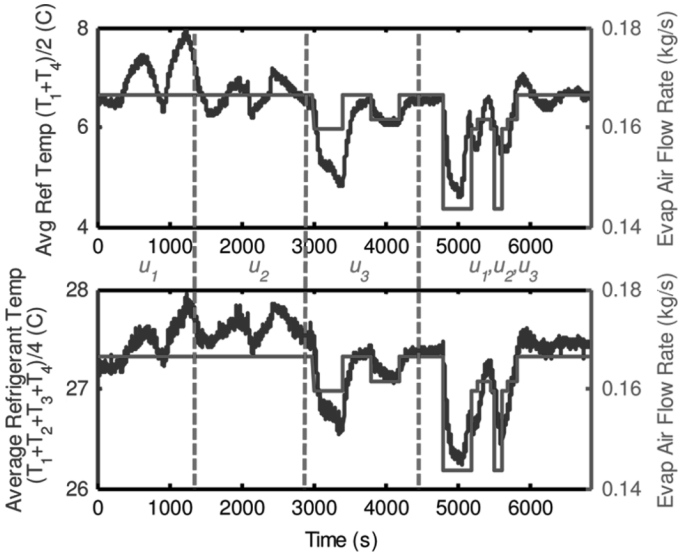

Fig. 12. Open-loop response t of I/O coupling for input u_3.

TABLE IV
INCIDENCE OF CANDIDATE OUTPUT PAIRINGS FOR u_3 FOR TOP 1000 PAIRINGS

Frequency	$T_{1+2+3+4}$	T_{1+3+4}	T_{1+4}	T_{1+2+4}
ω=0 rad/s	11%	8%	6%	6%
ω=0.01 rad/s	18%	9%	4%	7%

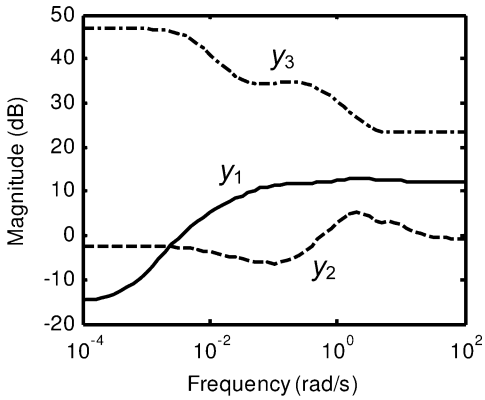

Fig. 13. RGA number frequency plot.

TABLE V
CANDIDATE I/O SETS

Inputs	Set y_1	Set y_2	Set y_3
u_1	P_3	P_{3+4}	T_{1-4}
u_2	P_{3-4}	P_{3-4}	P_4
u_3	T_{1+4}	T_{1+4}	$T_{e,air}$

The third set y_3 represents the I/O pairings commonly used in industry. Fig. 13 shows the RGA number for each I/O set as a function of frequency.

Sets $y_1(=[P_3, P_{3-4}, T_{1+4}])$ and $y_2(=[P_{3+4}, P_{3-4}, T_{1+4}])$ present a tradeoff in the RGA number. That is, set y_1 has a smaller RGA number at low frequencies whereas y_2 offers a smaller RGA number at higher frequencies. Set $y_3(=[T_{1-4}, P_4, T_{e,\text{air}}])$ has a significantly higher RGA number across all frequencies than both sets y_1 and y_2.

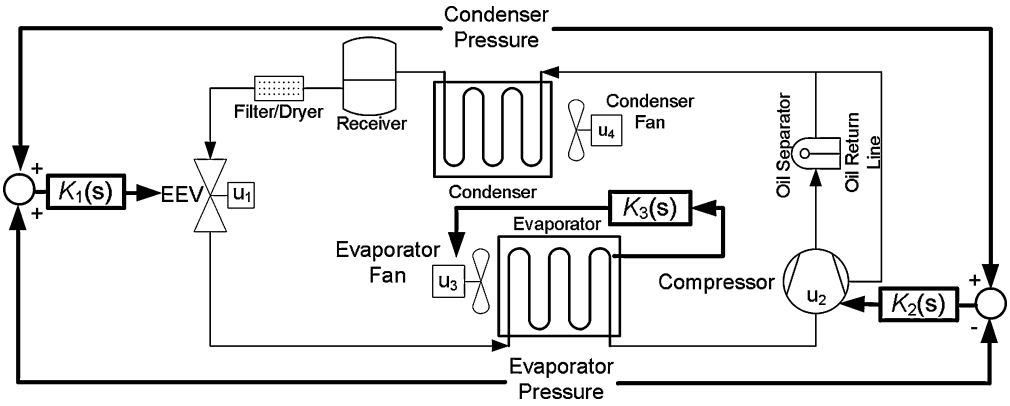

Fig. 14. Control approach for vapor compression systems with set y_2.

V. Comparison of Decentralized Controller Feedback Configurations

To further demonstrate system performance with the chosen I/O pairings, we compare sets y_2 and y_3 by designing decentralized PID controllers, composed of three individual SISO control loops, for each I/O set. The reference tracking characteristics of the controllers are evaluated on the experimental system. In order to reduce the number of I/O sets for comparison, we chose set y_2 although a similar analysis can be done with set y_1. As noted before, a tradeoff exists between sets y_1 and y_2. Specifically, the lower RGA number near the closed-loop bandwidth (from 10^{-3} to 10^{1} rad/s in Fig. 13) suggests that decentralized controllers tuned for set y_2 will result in a better transient performance on the experimental system which agrees with pairing rule 1 in [10]. The system performance at low frequencies with the I/O set y_1 was validated by experiments and is not detailed here.

The decentralized feedback configuration with I/O set y_2 on the experimental system is shown in Fig. 14. $K_1(s)$, $K_2(s)$, and $K_3(s)$ represent a PID controller for each individual loop, respectively. PID controllers are used here since they are commonplace in industrial applications due to their ease of implementation as discussed in [10], Sec. 10.5.1. The feedback configuration with I/O set y_3 is similar to that in Fig. 14 except for a difference in output variables.

The gains for each PID controller were first developed in simulation using an identified model for each I/O set. However, because of discrepancies between the model and the actual system, these PID gains were further turned directly on the experimental system. The tuning process was manual and based on user experience. Disturbance rejection was used to verify that both controllers were well tuned; these results are presented in detail in Appendix B. The tuned gains of the three SISO controllers for each I/O set (y_2 and y_3)) are given in Table VI. The different output variables that the EEV controls for I/O set y_2 versus set y_3 explains the difference in the magnitude of controller $K_1(s)$ gains.

Figs. 15 and 16 show the performance of the controlled experimental system for reference tracking with each I/O set, respectively. Note that similar operating conditions are used, and the reference commands for I/O set y_3 are an appropriate translation of the reference commands used for I/O set y_2. In Fig. 15,

TABLE VI
Tuned Gains for Three Controllers

Controller	set y_2			set y_3		
	P	I	D	P	I	D
$K_1(s)$	0.295	0.002	4	3	0.025	10
$K_2(s)$	17.5	0.55	3	17	0.55	8
$K_3(s)$	2.84	0.028	60	7	0.03	35

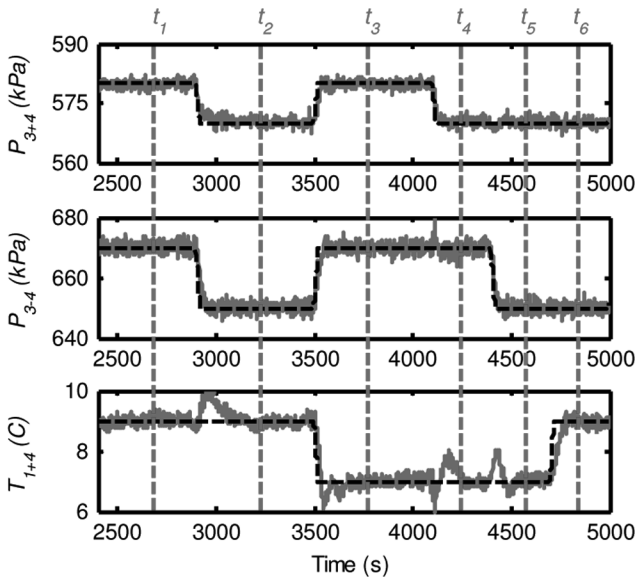

Fig. 15. Reference tracking with set y_2 feedback controller.

the P_{3+4} controller $K_1(s)$ and P_{3-4} controller $K_2(s)$ have a settling time of about 60 s, and the oscillation around the pressure set points is within ± 2 kPa. The T_{1+4} feedback controller $K_3(s)$ tracks the average temperature's change within $\pm 1^{\circ}$C error during the entire time period. In Fig. 16, the T_{1-4} controller is able to track the step change reference in evaporator superheat within $\pm 1^{\circ}$C error, while the P_4 controller struggles to track the evaporator pressure reference signal. There are persistent oscillations (as large as 10 kPa) around the pressure set point as a result of the strongly coupled system dynamics. Similarly, the $T_{\mathrm{e,air}}$ controller oscillates significantly around the air temperature set point, and the overshoot is as high as 100%.

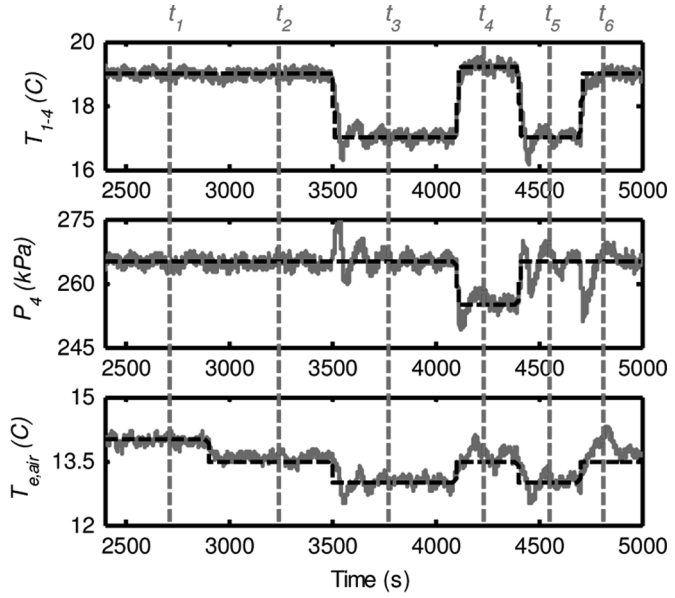

Fig. 16. Reference tracking with set y_3 feedback controller.

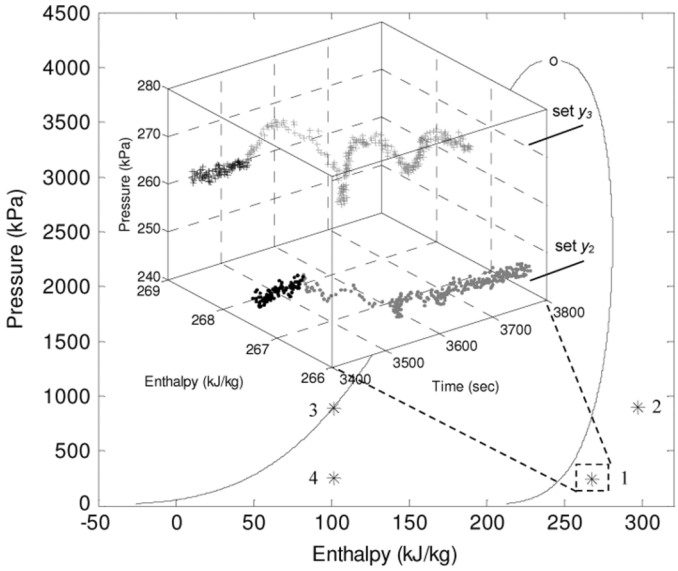

Fig. 17. Comparison of system transient performance with set y_2 against that with set y_3 controller.

Additional physical insight can be extracted from the reference commands shown in Fig. 15 with the controller for set y_2. During the time period t_1–t_2, the condenser pressure was decreased while maintaining a constant evaporator superheat. This results in an increase in COP by both decreasing the work done by the compressor and increasing the evaporator capacity.

The 3-D plot in Fig. 17 shows the system transient performance at the evaporator outlet with I/O sets y_2 and y_3 during time period t_2–t_3. Both controllers were used to track a step change in evaporator superheat while maintaining a constant evaporator pressure. Note that the step change in superheat is characterized by a step change in enthalpy in Fig. 17. It is apparent that the feedback controller for set y_2 maintains the pressure very well while tracking the step change in superheat. This is in contrast to the controller for set y_3 which causes the evaporator pressure to oscillate significantly during the step change in superheat.

These results emphasize that better performance can be obtained through the indirect control of a thermodynamic state of the system, in this case, evaporator pressure, with set y_2, rather than by directly controlling the state with set y_3. A step change in each output was successfully tracked in time periods t_3–t_4, t_4–t_5, and t_5–t_6, respectively. The results demonstrate that it is possible to design an optimization routine (recall Fig. 3) to meet desired performance objectives by leveraging the decoupled controllers to control each of the states in the thermodynamic cycle.

VI. Conclusion

In this paper, an extended set of unconventional I/O control pairings was analyzed using the RGA number to quantify the degree of coupling associated with any given I/O set. Although somewhat counterintuitive, the decrease in dynamic coupling which resulted from the best set allowed for an effective SISO control of the experimental system. Moreover, rather than explicitly controlling capacity or efficiency, the three individual SISO control loops were used to control specific thermodynamic states of the system as they relate to an idealized P–h diagram. The experimental results showed that a decentralized control approach pairing the EEV with average system pressure, the compressor speed with differential pressure, and the evaporator fan with average evaporator temperature resulted in a better reference tracking of each output. The results also confirmed the ability of three SISO controllers, designed with I/O set y_2, to independently track three set points. This suggested that, by merging a thermodynamic perspective with the control architecture of the system, a higher level planning algorithm can be used to optimize the set points for each state such that desired performance and efficiency objectives can be met.

Appendix A

The identified state-space $[\mathbf{A}, \mathbf{B}, \mathbf{C}, \mathbf{D}]$ system model for the two output pressures is given in (6), as shown at the top of the next page. Note that differential pressure, rather than P_2, was used for the identification.

The identified state-space $[\mathbf{A}, \mathbf{B}, \mathbf{C}, \mathbf{D}]$ system model for the four output temperatures is given in (5) and (6).

$$A = \begin{bmatrix} -0.005223 & -0.001279 & -0.001931 & -0.001775 \\ 0.004297 & -0.009974 & -0.0008009 & -0.01045 \\ 0.002392 & -0.01216 & -0.02788 & 0.01419 \\ 0.008754 & -0.03764 & -0.008403 & -0.09967 \end{bmatrix}$$

$$B = \begin{bmatrix} -0.0002653 & -1.441 \times 10^{-6} & 0.02306 \\ 0.000358 & -1.092 \times 10^{-5} & -0.02201 \\ 0.0006409 & -3.999 \times 10^{-6} & 0.1569 \\ 0.001668 & -7.543 \times 10^{-5} & -0.1625 \end{bmatrix}$$

$$C = \begin{bmatrix} 70.4 & -4.59 & 6.996 & -1.378 \\ -21.79 & 11.08 & 9.693 & 1.788 \\ -13.7 & -19.41 & 6.834 & -0.3643 \\ -12.24 & 0.6604 & 4.254 & -6.524 \end{bmatrix}$$

$$D = \begin{bmatrix} 0 & 0 & 0 \\ 0 & 0 & 0 \\ 0 & 0 & 0 \\ 0 & 0 & 0 \end{bmatrix}$$

$$\mathbf{u} = \begin{bmatrix} a_v & \omega_c & \dot{m}_{\text{air}} \end{bmatrix}^{\mathrm{T}} \qquad \mathbf{y} = \begin{bmatrix} T_1 & T_4 & T_2 & T_3 \end{bmatrix}^{\mathrm{T}}. \quad (5)$$

$$A = \begin{bmatrix} -0.06794 & 0.04704 & 0.2834 & -0.0481 & 0.2248 & 1.042 \\ -0.05117 & -0.2241 & -0.03257 & -0.2986 & 1.154 & 1.587 \\ 0.2587 & -0.3095 & -1.295 & 0.05653 & -0.4164 & -3.854 \\ -0.245 & -0.22 & 0.7531 & -0.7526 & 2.883 & 6.105 \\ 0.6989 & -3.387 & -5.924 & -2.978 & -0.9685 & -5.691 \times 10^{-6} \\ -0.5499 & 0.8788 & 2.963 & 0.1192 & 0 & -1.327 \end{bmatrix}$$

$$B = \begin{bmatrix} -0.001744 & 4.635 \times 10^{-6} & 0.1389 \\ -0.002344 & -4.676 \times 10^{-5} & 0.2562 \\ 0.007939 & -3.87 \times 10^{-5} & -0.4873 \\ -0.01288 & -9.731 \times 10^{-6} & 0.9648 \\ 0.002021 & -0.0004335 & 0.7811 \\ -0.01574 & 0.0001202 & 0.8895 \end{bmatrix}$$

$$C = \begin{bmatrix} 256.3 & 93.39 & 14.05 & -51.34 & 0 & 0 \\ 95.29 & -237 & 49.71 & 68.76 & 0 & 0 \end{bmatrix}$$

$$D = \begin{bmatrix} 0 & 0 & 0 \\ 0 & 0 & 0 \end{bmatrix}$$

$$\mathbf{u} = [\, a_v \quad \omega_c \quad \dot{m}_{\text{air}} \,]^{\text{T}} \qquad \mathbf{y} = [\, P_1 \quad P_{2-1} \,]^{\text{T}}. \tag{6}$$

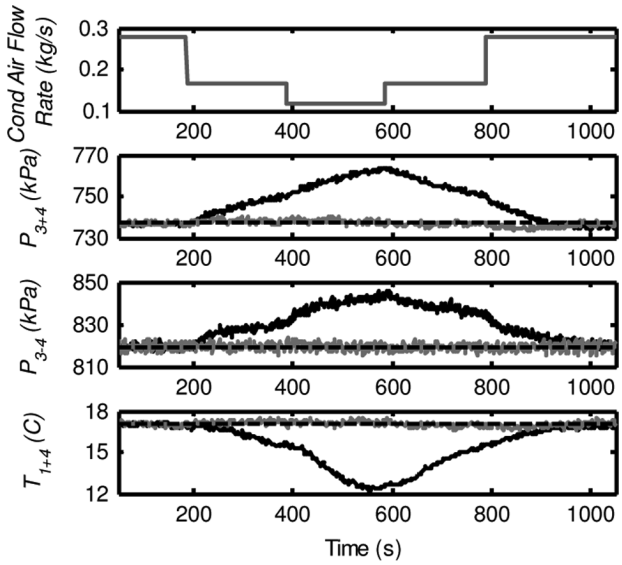

Fig. 18. Disturbance rejection by set y_2 feedback controller. Black and gray solid curves represent uncontrolled and controlled outputs, respectively.

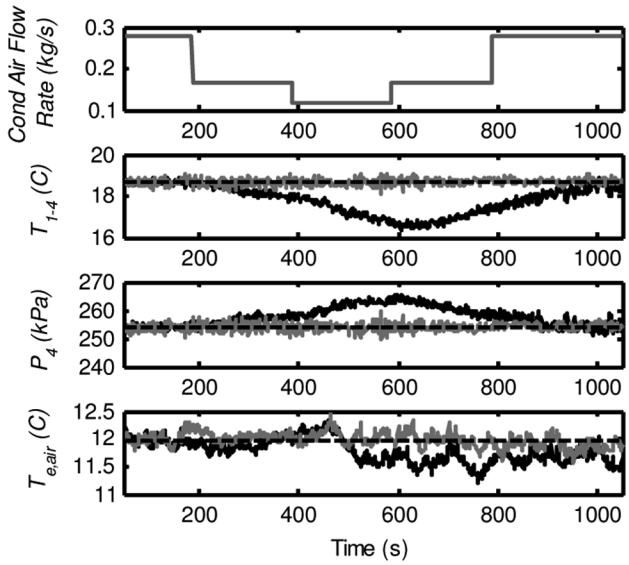

Fig. 19. Disturbance rejection by set y_3 feedback controller. Black and gray solid curves represent uncontrolled and controlled outputs, respectively.

APPENDIX B

To evaluate the controllers' disturbance rejection characteristics, changes in condenser-side airflow rate were used to apply a disturbance on the experimental system. The comparison between the closed- and open-loop system responses for I/O sets y_2 and y_3 are shown in Figs. 18 and 19, respectively. In spite of a significant disturbance applied to the system, as verified by the open-loop response, each controller successfully tracked their respective set points. This demonstrates that the controllers designed for I/O sets y_2 and y_3, respectively, are well tuned and have good disturbance rejection characteristics.

REFERENCES

[1] B. P. Rasmussen, "Dynamic modeling and advanced control of air conditioning and refrigeration systems," Ph.D. dissertation, Dept. Mech. Eng., Univ. Illinois Urbana–Champaign, Urbana, IL, 2005.

[2] X. D. He, S. Liu, and H. Asada, "Multivariable control of vapor compression systems," *HVAC&R Res.*, vol. 4, no. 3, pp. 205–230, Jul. 1998.

[3] R. Shah, B. Rasmussen, and A. Alleyne, "Application of multivariable adaptive control to automotive air conditioning systems," *Int. J. Adapt. Control Signal Process.*, vol. 18, no. 2, pp. 199–221, Mar. 2004.

[4] M. C. Keir, "Dynamic modeling, control, and fault detection in vapor compression systems," M.S. thesis, Dept. Mech. Eng., Univ. Illinois Urbana–Champaign, Urbana, IL, 2006.

[5] M. Keir and A. Alleyne, "Feedback structures for vapor compression cycle systems," in *Proc. Am. Control Conf.*, New York, Jul. 11–13, 2007, pp. 5052–5058.

[6] L. Larsen, C. Thybo, J. Stoustrup, and H. Rasmussen, "A method for online steady state energy minimization with application to refrigeration systems," in *Proc. 43rd IEEE CDC*, Nassau, Bahamas, Dec. 2004, pp. 4708–4713.
[7] J. B. Jensen and S. Skogestad, "Optimal operation of simple refrigeration cycles. Part II: Selection of controlled variables," *Comput. Chem. Eng.*, vol. 31, no. 12, pp. 1590–1601, Dec. 2007.
[8] L. Ljung, *System Identification Toolbox: For Use With Matlab*. Natick, MA: Math Works Inc., 2001.
[9] E. H. Bristol, "On a new measure of interaction for multi-variable process control," *IEEE Trans. Autom. Control*, vol. AC-11, no. 1, pp. 133–134, Jan. 1966.
[10] S. Skogestad and I. Postlethwaite, *Multivariable Feedback Control*. New York: Wiley, 1996.
[11] SEI Electronic Expansion Valves Sporlan Valve Company. Washington, MO, Jul. 2000, Bulletin 100-20.
[12] B. Rasmussen and A. Alleyne, "Gain scheduled control of an air conditioning system using the Youla parameterization," in *Proc. Am. Control Conf.*, Minneapolis, MN, Jun. 14–16, 2006, pp. 5336–5341.